Spin Disorder on a Triangular Lattice

Satoru Nakatsuji,[1]* Yusuke Nambu,[1] Hiroshi Tonomura,[1] Osamu Sakai,[1] Seth Jonas,[3] Collin Broholm,[3,4] Hirokazu Tsunetsugu,[2] Yiming Qiu,[4,5] Yoshiteru Maeno[1,6]

As liquids crystallize into solids on cooling, spins in magnets generally form periodic order. However, three decades ago, it was theoretically proposed that spins on a triangular lattice form a liquidlike disordered state at low temperatures. Whether or not a spin liquid is stabilized by geometrical frustration has remained an active point of inquiry ever since. Our thermodynamic and neutron measurements on $NiGa_2S_4$, a rare example of a two-dimensional triangular lattice antiferromagnet, demonstrate that geometrical frustration stabilizes a low-temperature spin-disordered state with coherence beyond the two-spin correlation length. Spin liquid formation may be an origin of such behavior.

Electronic magnetic moments (spins) in magnets generally develop periodic order at low temperatures. When such order is suppressed, however, qualitatively new quantum phases can emerge. For example, quantum spin liquids appear in quasi–one-dimensional spin chains when fluctuations enhanced by low dimensionality destabilize static correlations (*1*). In higher dimensions, magnetic order may also be suppressed because of the geometry of the crystal lattice. Such an effect occurs, for example, in an antiferromagnet with a structure formed by arrays of triangles. Antiferromagnetically interacting spins on the vertices of triangles cannot simultaneously satisfy all pairwise interactions and may remain disordered well below the conventional ordering scale set by the Weiss temperature, θ_W (*2*). Thus, "geometrical frustration" promotes high degeneracy among competing low-temperature phases, enhances quantum fluctuations, and may lead to unconventional quantum phenomena.

In two dimensions, the simplest form of a geometrically frustrated lattice is a triangular lattice with a single magnetic atom per unit cell. This is the system for which a quantum spin-disordered state in more than one dimension was first proposed more than three decades ago (*3*). Since then, extensive theoretical and experimental research has been carried out in pursuit of novel ground states without magnetic order in two dimensions. Although it is now believed that triangular lattice antiferromagnets with nearest-neighbor coupling exhibit 120° spin order (*4*–*6*), recent theories suggest that interactions beyond nearest-neighbor exchange, such as longer range and multiple-spin exchange interactions, may lead to a quantum spin-disordered ground state (*7*, *8*). Experimentally, however, only a few candidates for spin-disordered states in two dimensions have been reported, in an organic material with a distorted triangular lattice (*9*), in Kagomé-related antiferromagnets (*10*, *11*), and in a low-density solid ^{3}He film absorbed on a graphite surface (*12*). So far unanswered is the question of whether an insulating bulk solid with an exact triangular lattice of well-defined localized moments can exhibit a novel ground state without magnetic order.

We demonstrate that high-quality samples of $NiGa_2S_4$, a bulk-insulating antiferromagnet on an exact triangular lattice, exhibit a spin-disordered state in two dimensions. Despite strong antiferromagnetic (AF) interactions, no magnetic long-range order was observed down to 0.35 K, where we instead found nanoscale quasi-static correlation. The spin-disordered state appeared on cooling through highly degenerate states with an entropy plateau and exhibited gapless, linearly dispersive modes, suggesting coherence beyond the two-spin correlation length. The gapless excitations were insensitive to a magnetic field but sensitive to impurities. These observations indicate the absence of canonical spin glass freezing in the bulk, raising the possibility of a spin liquid state with slow dynamics.

$NiGa_2S_4$ is a layered chalcogenide magnetic insulator with a stacked triangular lattice of Ni spins (*13*) (Fig. 1A). The structure is highly two-dimensional (2D) and the central NiS_2 layer is isostructural with the CoO_2 layer in superconducting $Na_xCoO_2{\cdot}yH_2O$ (*14*). Magnetism is associated with Ni^{2+} with the electronic configuration $t_{2g}^6 e_g^2$ and spin $S = 1$. The unit cell contains a single Ni^{2+} atom, so the intra- and inter-plane Ni separations are simply given by the lattice parameters $a = 0.3624$ nm and $c = 1.1999$ nm.

In Fig. 2A, the temperature dependence of the magnetic susceptibility, $\chi(T) \equiv M(T)/B$, and its inverse, $\chi^{-1}(T)$, where T is the temperature, are presented. The applied field B

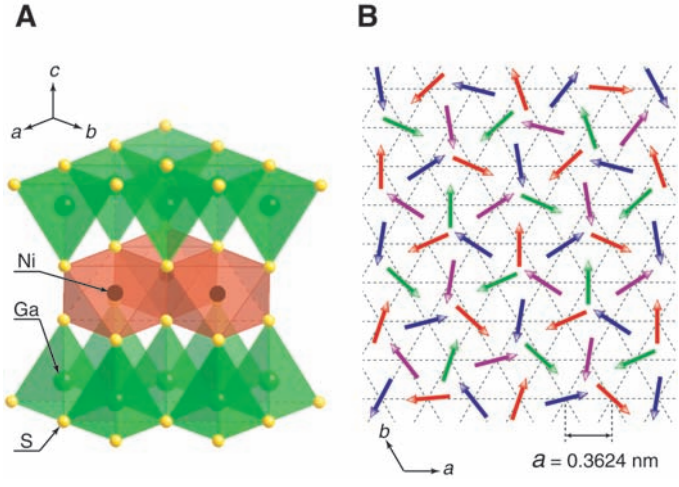

Fig. 1. Crystal and spin structures of $NiGa_2S_4$. (**A**) The slab structure of $NiGa_2S_4$ consists of a central NiS_2 layer of edge-sharing NiS_6 octahedra (red) and top and bottom sheets of GaS_4 tetrahedra (green). The slabs are stacked along the *c* axis and separated from each other by a van der Waals gap. Polycrystalline samples of $NiGa_2S_4$ were synthesized by heating the mixture of elements Ni, Ga, and S in evacuated silica ampoules at 900°C. Our powder x-ray measurements at room temperature and neutron diffraction measurements in the temperature range 1.5 K to 300 K confirmed that $NiGa_2S_4$ retains the trigonal crystal structure down to 1.5 K with $P\bar{3}m1$ symmetry. The refinements are consistent with the room-temperature structure (*13*). (**B**) The short-range correlated spin structure on the triangular Ni lattice, including the incommensurability observed by magnetic neutron diffraction. It approximates four independent 120° structures on the colored sublattices with lattice parameters 2*a*. The in-plane correlation length is 2.5(3) nm, and the correlation time exceeds 0.3 ns. There are weak ferromagnetic correlations between nearest-neighbor planes.

[1]Department of Physics, [2]Yukawa Institute for Theoretical Physics, Kyoto University, Kyoto 606-8502, Japan. [3]Department of Physics and Astronomy, Johns Hopkins University, Baltimore, MD 21218, USA. [4]NIST Center for Neutron Research, National Institute of Standards and Technology (NIST), Gaithersburg, MD 20899, USA. [5]Department of Materials Science and Engineering, University of Maryland, College Park, MD 20742, USA. [6]International Innovation Center, Kyoto University, Kyoto 606-8501, Japan.

*To whom correspondence should be addressed. E-mail: nakatsuji@scphys.kyoto-u.ac.jp

was 7 T, a field at which the magnetization M remains proportional to B. No difference was found between field-cooled and zero field-cooled data. Susceptibility above 150 K followed the Curie-Weiss law: $\chi^{-1}(T) = (T - \theta_W)/C$, and the Curie constant C corresponds to an effective moment of 2.81(3) Bohr magnetons (μ_B), consistent with spin-1 ($S = 1$) Ni^{2+}. The Weiss temperature, $\theta_W = -80(2)$ K, indicates strong AF interactions. However, in a field of 7 T, no sharp magnetic anomaly or field hysteresis was observed down to 1.8 K. Instead, the susceptibility smoothly increased on cooling and passed through a shallow and broad maximum at $T \sim 10$ K before approaching a finite low-T limit. These data exclude the possibility of a conventional spin-gap system in which the susceptibility vanishes exponentially at low temperatures.

Specific heat data, $C_p(T)$, also showed no evidence of a phase transition for fields between 0 T and 7 T and temperatures from 175 K down to 0.35 K (Fig. 2B, inset). These data indicate a disordered low-temperature state without conventional AF order. We probed the density of states for spin excitations through the magnetic specific heat $C_M(T)$ after subtraction of the lattice contribution (*15*). $C_M(T)$ (Fig. 2B) exhibited an unusual double-peak structure. One peak was broad and centered around $T = |\theta_W|$, below which the susceptibility was suppressed compared to the one expected from the high-temperature Curie-Weiss law (Fig. 2A). The lower temperature peak featured a prominent rounded maximum at $T_{peak} \approx 10$ K, where $\chi(T)$ also showed a broad maximum. The entropy S_M, obtained through integration of C_M/T (Fig. 2B), correspondingly had a plateau at $S_M \approx \frac{1}{3} R\ln 3$ before high-T saturation at $S_M \approx R\ln 3$, where R is the gas constant. This indicates high degeneracy of low-energy states because of magnetic frustration and is similar to predictions for the spin-1/2 antiferromagnet on the Kagomé lattice of corner-sharing triangles (*16*).

The specific heat exhibited power-law behavior at low temperatures (Fig. 3). The data between 0.35 and 4.0 K are well fitted by a power law $C_M = AT^{\alpha}$, where A is a constant and α is 2.001(5) (Fig. 3A). Quadratic temperature dependence through one decade indicates the presence of gapless and linearly dispersive modes in two dimensions. A gapless spectrum is furthermore consistent with a finite value of the susceptibility in the low-T limit. If the low-T specific heat peak were associated with AF ordering of individual $S = 1$ spins, it would be suppressed under a magnetic field of $k_B T_{peak}/g\mu_B \sim 7$ T, where k_B is the Boltzmann constant and g is the g factor. Instead, the specific heat was unaffected by fields up to 7 T, indicating that the low-T peak reflects short-range correlations among composite degrees of freedom that do not directly couple to a uniform field (*17*). It follows that the linearly dispersive excitations implied by $C_M \propto T^2$ are collective modes of moment-free spin clusters. Likewise, the specific heat peak at high $T \sim |\theta_W|$ and the concomitant suppression of the susceptibility compared to the one expected from high-temperature Curie-Weiss law are attributable to the formation of incoherent moment-free spin clusters. Similar thermodynamic properties have been reported for the Kagomé-related antiferromagnets, $SrCr_{9p}Ga_{12-9p}O_{19}$ (*10*, *17*), and for deuteronium jarosite (*11*).

Although no susceptibility anomaly was observed at 7 T, weak field dependence and hysteresis was observed at low fields for temperatures below a freezing temperature $T_f = 8.5$ K (Fig. 3B). Previous work indicates that minute levels of quenched disorder can induce spin freezing in geometrically frustrated magnets (*2*). However, the bifurcation of $\chi(T)$ in $NiGa_2S_4$ is distinct from previous observations in frustrated magnets in that it involves only a small component of the whole susceptibility

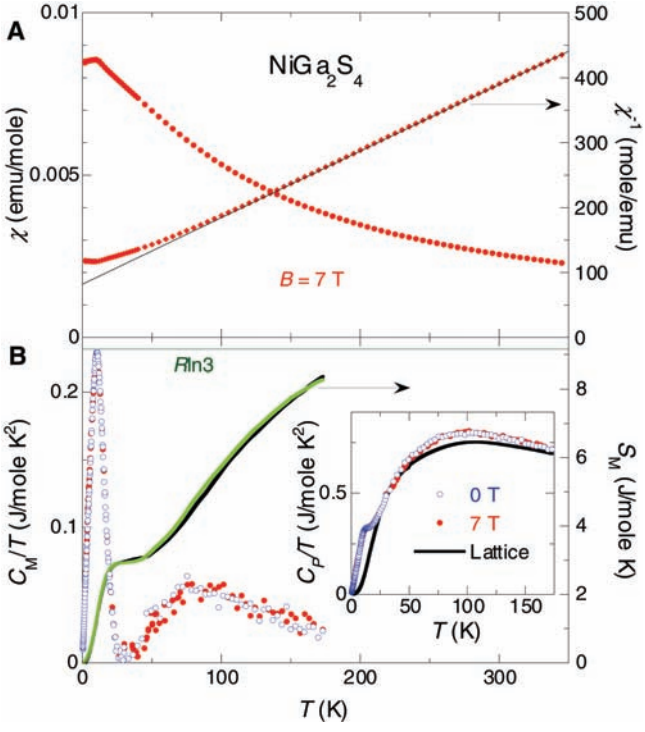

Fig. 2. Temperature dependence of the susceptibility and specific heat of polycrystalline $NiGa_2S_4$. (**A**) The susceptibility χ (circles, left axis) and inverse susceptibility χ^{-1} (diamonds, right axis), measured at 7 T with a superconducting quantum interference device (SQUID) magnetometer (Quantum Design, model MPMS-XL). The solid line is the Curie-Weiss fit. emu, electromagnetic unit. (**B**) The magnetic part of the specific heat divided by temperature C_M/T (left axis) at zero field (blue open circles) and at 7 T (red solid circles) and the entropy S_M (right axis) at 0 T (green line) and at 7 T (black line). The horizontal line indicates $S_M = R\ln 3$. Inset: C_p/T for $NiGa_2S_4$ at 0 T (blue open circles) and 7 T (red solid circles) and its lattice part C_L/T [black solid line (*15*)].

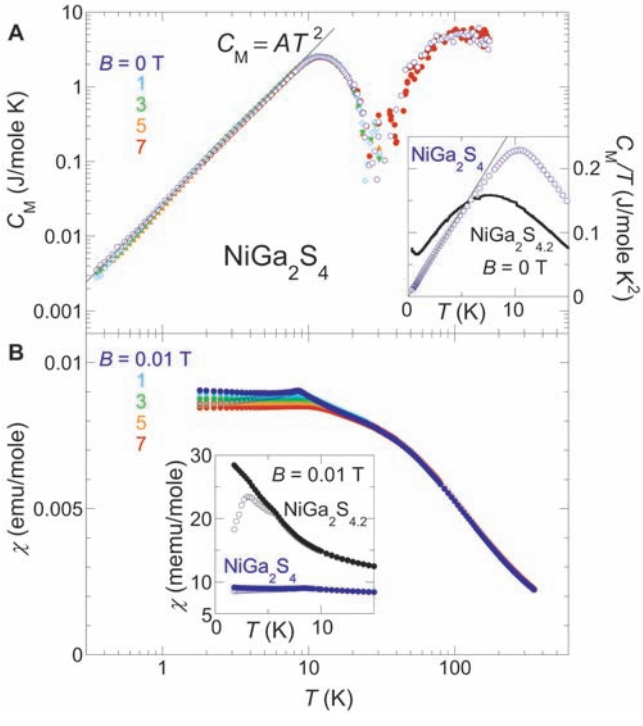

Fig. 3. Magnetic field dependence of the specific heat and susceptibility of $NiGa_2S_4$. (**A**) The magnetic part of the specific heat C_M under different fields versus temperature in full logarithmic scale. Inset: C_M/T versus temperature under zero field for $NiGa_2S_4$ and the sample with nominal doping of excess 5% sulfur, $NiGa_2S_{4.2}$. The solid lines show the T^2 dependence of C_M. (**B**) The susceptibility χ under different fields. Inset: The low-temperature part of χ for $NiGa_2S_4$ and $NiGa_2S_{4.2}$ at 0.01 T. Both field-cooled (solid circles) and zero field-cooled (open circles) data are shown.

(~5%). The following observations indicate that it may in fact be a surface effect. First, intentional impurity doping by 5% excess sulfur leads to a substantial enhancement of freezing behavior (*18*). A large value of $C_M(T)/T$ (~70 mJ/mol K^2) was induced for $T \rightarrow 0$ and hysteresis in $\chi(T)$ was strongly enhanced (Fig. 3, inset). Second, when a field around the critical value $B_c \sim 7$ T was applied, the hysteretic part of the susceptibility completely disappeared, whereas the specific heat, $C_M(T)$, showed only negligible field dependence in the same B-T range. Because magnetism is extremely sensitive to imperfection, the different field effects of the two thermodynamic quantities, together with $C_M(T)/T \rightarrow 0.0(1)$ mJ/mol K^2 as $T \rightarrow 0$ K, indicate that the hysteretic part of the susceptibility is associated with a very small density of impurities. In addition, the value of B_c implies that impurity spins are individual $S = 1$ objects, as this value agrees with the magnetic field where $S = 1$ impurity spins become polarized, $B_c \sim k_B T_f / g\mu_B$. Third, the density of spins involved in freezing can be estimated from the difference between $\chi(T)$ for $B = 0$ T and 7 T, which follows a Curie-Weiss law with $\theta_W = 9$ K and an effective moment corresponding to 300 parts per million (ppm) of the Ni sites. This concentration matches that of surface spins in the ~10 μm^3 grains of our sample. Finally, this small density of impurities is consistent with diffraction measurements. No trace of disorder or impurities was found by x-ray or neutron powder diffraction, and Rietveld refinement of neutron powder diffraction data is consistent with the nominal stoichiometry.

To investigate low-energy spin correlations, we performed a magnetic neutron scattering experiment (*19*). Figure 4 shows the difference in elastic powder neutron scattering between T = 1.5 K and 15 K. The signal was resolution-limited in energy [$\delta E = 0.10$ meV, where δE is full width at half maximum (FWHM) energy resolution], which allows us to conclude that the correlations persist on a time scale that exceeds 0.3 ns. The absence of a difference signal in the $Q \rightarrow 0$ limit, where Q is the scattering wave vector, indicates a correlated state built from moment-free spin clusters. Classical spins on a triangular lattice with nearest-neighbor AF interactions should develop correlations of the 120° variety with wave vector $\boldsymbol{q} = (\frac{1}{3}, \frac{1}{3}, 0)$. $NiGa_2S_4$ exhibited a peak at $Q_M = 0.57(1)$ Å$^{-1} \approx 2\pi/3a = 0.5779$ Å^{-1}, which is the length of $\boldsymbol{q} = (\frac{1}{6}, \frac{1}{6}, 0)$. To understand this result, we compared the data to the spherical average of magnetic scattering from a quasi-2D magnet:

$$\frac{\partial\sigma}{\partial\Omega} = r_0^2 \left|\frac{g}{2}F(Q)\right|^2 N \sum_{\tau} \left(|m_{\boldsymbol{q}}|^2 - |\hat{\boldsymbol{Q}} \cdot m_{\boldsymbol{q}}|^2\right) \times [1 + 2\alpha \cos(\boldsymbol{Q} \cdot \boldsymbol{c})] \frac{A^* \kappa^2/\pi}{[(\boldsymbol{Q} - \tau \pm \boldsymbol{q})^2 + \kappa^2]^2} \quad (1)$$

Here σ is the scattering cross section, Ω is the solid angle of detection, $r_0 = 5.4 \times 10^{-15}$ m, F is the magnetic form factor for Ni^{2+}, N is the number of magnetic ions, A^* is the area of the Brillouin zone, and the summation is over 2D reciprocal lattice vectors τ. The spin expectation value on site, r, averaged over a time interval that exceeds 0.3 ns, is given by $\langle \boldsymbol{S}_r \rangle = \boldsymbol{m}_{\boldsymbol{q}} e^{i\boldsymbol{q}\cdot\boldsymbol{r}} + \boldsymbol{m}_{\boldsymbol{q}}^* e^{-i\boldsymbol{q}\cdot\boldsymbol{r}}$, where $\boldsymbol{m}_{\boldsymbol{q}}$ is a complex vector. In Eq. 1, κ is the inverse 2D correlation length and $\alpha = \langle \boldsymbol{S}_0 \cdot \boldsymbol{S}_{\pm\boldsymbol{c}} \rangle \langle \boldsymbol{S}_0 \cdot \boldsymbol{S}_0 \rangle^{-1}$ represents nearest-neighbor inter-plane correlations. When $\boldsymbol{q}$ was not $(\frac{1}{3}, \frac{1}{3}, 0)$, there were three symmetry-related wave vector domains. The line in Fig. 4 corresponds to $\boldsymbol{q} = (\eta, \eta, 0)$ with $\eta = 0.158(1)$ and $\boldsymbol{m}_{\boldsymbol{q}} = \hat{\boldsymbol{x}}\, m_{\boldsymbol{q}x} + i\hat{\boldsymbol{y}} m_{\boldsymbol{q}y} + \hat{\boldsymbol{z}} m_{\boldsymbol{q}z}$, where $m_{\boldsymbol{q}x} = 0.31(3)$, $m_{\boldsymbol{q}y} = 0.43(4)$, and $m_{\boldsymbol{q}z} = 0.0(1)$. Here $\hat{\boldsymbol{z}} \parallel \boldsymbol{c}$ and $\hat{\boldsymbol{x}}$, $\hat{\boldsymbol{y}}$ are parallel and perpendicular to $\boldsymbol{q}$, respectively. The corresponding time- and site-averaged spin is $|\langle S \rangle| = \sqrt{(1/N \sum_{\boldsymbol{r}} \langle \boldsymbol{S}_r^2 \rangle)} = \sqrt{2}|\boldsymbol{m}_{\boldsymbol{q}}| = 0.75(8)$. This value is notably reduced from $S = 1$ for Ni^{2+} because of quantum fluctuations enhanced by frustration and low dimensionality. It is also important that the in-plane correlation length, $\xi = \kappa^{-1} = 2.5(3)$ nm, corresponds to 6.9(8) triangular lattice spacings and ~2.5×10^{-4} times the powder sample grain size. Ferromagnetic inter-plane correlations were limited to nearest neighbors as indicated by $\alpha = 0.25(5)$.

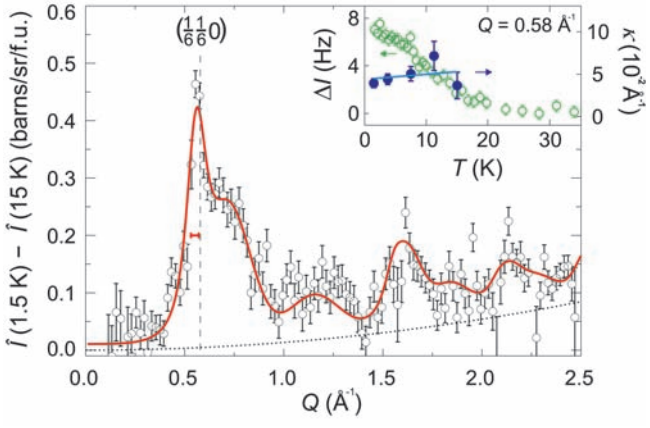

Fig. 4. The difference between elastic powder neutron scattering from $NiGa_2S_4$ at T = 1.5 K and 15 K. The solid line is calculated for the quasi-2D spin structure shown in Fig. 1B. The horizontal red bar under the peak indicates the FWHM resolution width. Green circles in the inset show the elastic scattering intensity difference $\Delta I = I(T) - I(50\ \text{K})$ at the wave vector transfer $Q = 0.58$ Å^{-1}, as probed with FWHM energy resolution $\delta E = 0.36$ meV. Solid blue symbols in the inset show the inverse correlation length, κ, inferred from fitting the difference data. The fits include a ~Q^2 term in the intensity (dashed line) to account for temperature-dependent nuclear incoherent scattering. f.u., formula unit.

The incommensurate short-range order inferred from the diffraction data (Fig. 1B) has various possible explanations. If third-neighbor AF interactions, J_3, dominate, magnetic orders with $\boldsymbol{q} = (\frac{1}{6}, \frac{1}{6}, 0)$ and/or $(\frac{1}{3}, \frac{1}{3}, 0)$ will be degenerate at the mean field level. Nearest neighbor couplings, J_1, lift the degeneracy. When J_1 is ferromagnetic, a $(\frac{1}{6}, \frac{1}{6}, 0)$ order is favored, but the wave vector will be shifted to an incommensurate value (η, η, 0), as in our diffraction data. From the experimental value of $\eta = 0.158(1)$, mean field theory yields $J_1/J_3 = -0.2(1)$. Indeed, because the nearest-neighbor Ni-S-Ni bond angle was near 90°, J_1 should be small and potentially ferromagnetic. Alternatively, proximity of the NiS_2 layer to a metal-insulator transition may produce multiple-spin exchange that stabilizes a larger unit cell.

Although the spin correlation length, $\xi = 2.5(3)$ nm, is rather short, specific heat data indicate a much longer coherence length for low-energy excitations. When coherent propagation of excitations is limited up to a length scale L_0 at $T = 0$, the specific heat deviates from the low-T asymptotic form as $C_M/R = -(\sqrt{3}\pi/2)(a/L_0)^2 + [3\sqrt{3}\zeta(3)/2\pi](ak_BT/\hbar D)^2$ at $hD/(L_0k_B) \ll T \ll \theta_W$, where D is the spin stiffness constant (*20*). Least-squares fitting of this expression to the specific heat data in Fig. 3 yields a lower bound, $L_0 > 200$ nm. Clearly, this is far greater than the two-spin correlation length, $\xi = 2.5(3)$ nm, determined by neutron diffraction, and it indicates that coherent low-energy modes are a bulk effect in $NiGa_2S_4$.

These experimental results demonstrate that $NiGa_2S_4$ has unique low-temperature properties: (i) absence of conventional magnetic order, which is replaced by incommensurate short-range order with nanoscale correlation; (ii) absence of canonical bulk spin glass freezing; (iii) gapless coherent excitations in two dimensions that are insensitive to field but sensitive to impurities; and (iv) highly degenerate low-energy states as indicated by an entropy plateau. These observations place strong constraints on possible ground states. One likely candidate is a spin liquid with no conventional magnetic long-range order as characterized by resolution-limited Bragg peaks, no static spin freezing, and an absence of spin dimerization (i.e., valence bond solid order) that would induce a finite spin gap. Observations (i), (ii), and (iii) are consistent with these criteria. Moreover, observations (iii) and (iv) are consistent with the type of spin liquid that is expected to result from quantum effects in a highly degenerate manifold induced by mag-

netic frustration. For example, recent theoretical work on the single-band Hubbard model on the triangular lattice suggests that a gapless spin liquid phase is realized at intermediate correlations (*8*). It is also predicted that the spin liquid phase has both spin-zero and nonzero low energy excitations (*21*) and incommensurate short-range correlation (*22*), which may be related to these observations.

Another possibility is a delicate form of long-range order that is dynamically inaccessible in real materials because of impurity pinning close to quantum criticality. Other possible ground states include a Kosterlitz-Thouless (KT) phase driven by two-valued vortices with the transition around T_{peak} (*23*) and a long-range order without long-range spin correlations such as in a spin nematic (*24*). The KT phase discussed here is not a conventional one but has a finite spin-correlation length, consistent with our observations. The neutron scattering data show that a large part of the magnetic spectral weight is associated with a long time scale that exceeds 0.3 ns. Experiments characterizing slow spin dynamics are in progress to distinguish between these exotic potential ground states in $NiGa_2S_4$.

Like the spin-1/2 chain in one dimension (*1*), the triangular lattice antiferromagnet, which is the only geometrically frustrated 2D Bravais lattice, plays a central role in the search for cooperative phenomena in two dimensions. With AF nearest-neighbor interactions, Ising spins have residual entropy (*25*), and classical Heisenberg spins have a KT-type transition and noncolinear Néel order at $T = 0$ (*23*). In the extreme quantum spin-1/2 case, a superposition of singlet coverings constituting a resonating valence bond state was first introduced to describe the ground state of the triangular lattice antiferromagnet (*3*). Although it is now believed that a nearest-neighbor Heisenberg spin-1/2 model has 120° order at $T = 0$ (*4*–*6*), one may expect various exotic phases in real materials, driven by other effects such as longer range interactions, multiple-spin exchange, and structural dimerization. Consequentially, there have been intensive experimental searches for an ideal quasi-2D triangular lattice antiferromagnet with a small spin quantum number ($S \leq 1$) (*26*). Several spin-1/2 triangular lattices have been reported to show nonordered gapless phases, but all the materials so far have either a distorted structure (*9*, *27*) or are only available in minute quantities, which limits accessibility for many experimental techniques (*12*).

To our knowledge, $NiGa_2S_4$ is the first low spin ($S \leq 1$), quasi-2D bulk magnet on an exact regular triangular lattice. Our measurements on $NiGa_2S_4$ demonstrate that geometrical frustration can be used to stabilize a spin-disordered state at low temperatures. A strongly fluctuating spin state has been discovered in a triangular lattice plane that is isostructural to the superconducting CoO_2 layer of $Na_xCoO_2{\cdot}yH_2O$ (*14*) and isostoichiometric with NiS_2, a metal-insulator transition system (*28*). It may thus be possible to drive $NiGa_2S_4$ into a conducting state in which the magnetic fluctuations have a qualitative effect on carrier correlations.

References and Notes

1. I. Affleck, *J. Phys. Condens. Matter* **1**, 3047 (1989).
2. A. P. Ramirez, in *Handbook of Magnetic Materials*, K. J. H. Buschow, Ed. (Elsevier Science, Amsterdam, 2001), vol. 13, pp. 423–520.
3. P. W. Anderson, *Mater. Res. Bull.* **8**, 153 (1973).
4. D. A. Huse, V. Elser, *Phys. Rev. Lett.* **60**, 2531 (1988).
5. B. Bernu, C. Lhuillier, L. Pierre, *Phys. Rev. Lett.* **69**, 2590 (1992).
6. L. Capriotti, A. E. Trumper, S. Sorella, *Phys. Rev. Lett.* **82**, 3899 (1999).
7. G. Misguich, C. Lhuillier, in *Frustrated Spin Systems*, H. T. Diep, Ed. (World-Scientific, Singapore, 2004), pp. 229–306.
8. H. Morita, S. Watanabe, M. Imada, *J. Phys. Soc. Jpn.* **71**, 2109 (2002).
9. Y. Shimizu, K. Miyagawa, K. Kanoda, M. Maesato, G. Saito, *Phys. Rev. Lett.* **91**, 107001 (2003).
10. A. P. Ramirez, G. P. Espinosa, A. S. Cooper, *Phys. Rev. Lett.* **64**, 2070 (1990).
11. A. S. Wills, A. Harrison, S. A. M. Mentink, T. E. Mason, Z. Tun, *Europhys. Lett.* **42**, 325 (1998).
12. K. Ishida, M. Morishita, K. Yawata, H. Fukuyama, *Phys. Rev. Lett.* **79**, 3451 (1997).
13. H. D. Lutz, W. Buchmeier, H. Siwert, *Z. Anorg. Allg. Chem.* **533**, 118 (1986).
14. K. Takada *et al.*, *Nature* **422**, 53 (2003).
15. The specific heat, C_P, was measured by a thermal relaxation method down to 0.35 K under fields up to 7 T. In order to estimate the lattice part of the specific heat, C_L, we measured C_P for the isostructural nonmagnetic analog $ZnIn_2S_4$ and obtained the thermal variation of the Debye temperature $\theta_D(T)$ using the Debye equation (*29*). $\theta_D(T)$ of $NiGa_2S_4$ was then estimated by applying a scale factor according to $\theta_D \propto M_0^{-1/2}V_0^{-1/3}$, where M_0 and V_0 are molar mass and volume, respectively. Finally, C_L was estimated by converting the scaled $\theta_D(T)$ data into specific heat. The magnetic part, C_M, was estimated as the difference between the total specific heat, C_P, and the lattice estimation C_L.
16. P. Sindzingre *et al.*, *Phys. Rev. Lett.* **84**, 2953 (2000).
17. A. P. Ramirez, B. Hessen, M. Winklemann, *Phys. Rev. Lett.* **84**, 2957 (2000).
18. J. Mydosh, *Spin Glasses: An Experimental Introduction* (Taylor and Francis, London, 1993).
19. Neutron diffraction experiments were performed on the Disc Chopper Spectrometer at NIST with 3.55-meV neutrons and an elastic energy resolution of 0.10 meV. Measurements versus T were carried out on the cold neutron triple axis spectrometer SPINS, with an energy of 5 meV and an energy resolution of 0.36 meV.
20. High degeneracy of low-temperature states is indicated not only by the large value of the entropy plateau at $S_M \approx {}^1/_3 R\ln 3$ at $T \sim 20$ K but also by the stiffness constant D. For ordinary antiferromagnets that order at $T \sim |\theta_W|$, the stiffness D_0 is estimated by the relation $D_0^2 \approx [3\sqrt{3}\zeta(3)/4\pi](ak_B\theta_W/\hbar)^2/\ln(2S + 1)$, with $\zeta(3) = 1.202$. In our case, the observed D was 850 m/s, nearly three times smaller than the expected D_0 of 2500 m/s, indicating softening due to magnetic frustration.
21. M. Imada, T. Mizusaki, S. Watanabe, available at http://arxiv.org/abs/cond-mat/0307022 (2003).
22. T. Kashima, M. Imada, *J. Phys. Soc. Jpn.* **70**, 3052 (2001).
23. H. Kawamura, S. Miyashita, *J. Phys. Soc. Jpn.* **53**, 4138 (1984).
24. P. Chandra, P. Coleman, *Phys. Rev. Lett.* **66**, 100 (1991).
25. G. H. Wannier, *Phys. Rev.* **79**, 357 (1950).
26. M. F. Collins, O. A. Petrenko, *Can. J. Phys.* **75**, 605 (1997).
27. K. Takeda, K. Miyake, K. Takeda, K. Hirakawa, *J. Phys. Soc. Jpn.* **61**, 2156 (1992).
28. J. A. Wilson, in *Metallic and Nonmetallic States of Matter*, P. P. Edwards, C. N. R. Rao, Eds. (Taylor and Francis, London, 1985), pp. 215–260.
29. J. A. Beattie, *J. Math. Phys.* **6**, 1 (1926/1927).

30. We thank J. Y. Chan, S. Fujimoto, K. Ishida, K. Kitagawa, R. T. Macaluso, D. E. MacLaughlin, R. Moessner, S. Sondhi, and O. Tchernyshyov for fruitful discussions. Work at Kyoto University supported in part by Grants-in-Aid for Scientific Research from the Japan Society for the Promotion of Science and for the 21st Century Center of Excellence "Center for Diversity and Universality in Physics" from the Ministry of Education, Culture, Sports, Science and Technology (MEXT) of Japan and by the Inamori Foundation. Work at Johns Hopkins University was supported by the U.S. Department of Energy.

11 May 2005; accepted 4 August 2005
10.1126/science.1114727

Conversion of Zinc Oxide Nanobelts into Superlattice-Structured Nanohelices

Pu Xian Gao,[1] Yong Ding,[1] Wenjie Mai,[1] William L. Hughes,[1] Changshi Lao,[1] Zhong Lin Wang[1,2,3]*

A previously unknown rigid helical structure of zinc oxide consisting of a superlattice-structured nanobelt was formed spontaneously in a vapor-solid growth process. Starting from a single-crystal stiff nanoribbon dominated by the *c*-plane polar surfaces, an abrupt structural transformation into the superlattice-structured nanobelt led to the formation of a uniform nanohelix due to a rigid lattice rotation or twisting. The nanohelix was made of two types of alternating and periodically distributed long crystal stripes, which were oriented with their *c* axes perpendicular to each other. The nanohelix terminated by transforming into a single-crystal nanobelt dominated by nonpolar $(01\bar{1}0)$ surfaces. The nanohelix could be manipulated, and its elastic properties were measured, which suggests possible uses in electromechanically coupled sensors, transducers, and resonators.

Helical structures have been observed for a number of inorganic materials. For example, carbon nanotube coils (*1*) are created when paired pentagon-heptagon atomic rings arrange themselves periodically within the hexagonal carbon network (*2*). Formation of nanosprings